A Two-fold Interpenetrated Zinc-Organic Framework: Luminescent Detection of $CrO_4^{2-}/Cr_2O_7^{2-}$ and Chemical Conversion of CO_2

Ying Shi,[a] Tian-Qun Song,[a,b] Chun-Shuai Cao[a] and Bin Zhao*[a]

[a.] *Department of Chemistry, Key Laboratory of Advanced Energy Material Chemistry, MOE, and Collaborative Innovation Center of Chemical Science and Engineering (Tianjin), Nankai University, Tianjin 300071, China.*
[b.] *Department of Chemistry, Tianjin University, Tianjin 300072, China*

Table S1. Crystal data and structure refinement for compound **1**.

Identification code	**1**
Empirical formula	$C_{23}H_{21.4}N_3O_{8.2}Zn$
Formula weight	536.44
Temperature/K	120.00(10)
Crystal system	triclinic
Space group	*P-1*
a/Å	10.1188(7)
b/Å	10.9420(11)
c/Å	11.7024(10)
α/°	63.853(9)
β/°	82.358(6)
γ/°	72.588(7)
Volume/Å^3	1109.81(18)
Z	2
ρ_{calc}g/cm^3	1.579
μ/mm^{-1}	1.164
F(000)	535.0
Radiation	MoKα (λ = 0.71073)
2Θ range for data collection/°	5.728 to 50.016
Index ranges	$-11 \le h \le 12$, $-12 \le k \le 13$, $-7 \le l \le 13$
Independent reflections	3894 [R_{int} = 0.0469, R_{sigma} = 0.0784]
Goodness-of-fit on F^2	0.941
Final R indexes [I>=2σ (I)]	R_1 = 0.0544, wR_2 = 0.1313
Final R indexes [all data]	R_1 = 0.0761, wR_2 = 0.1459

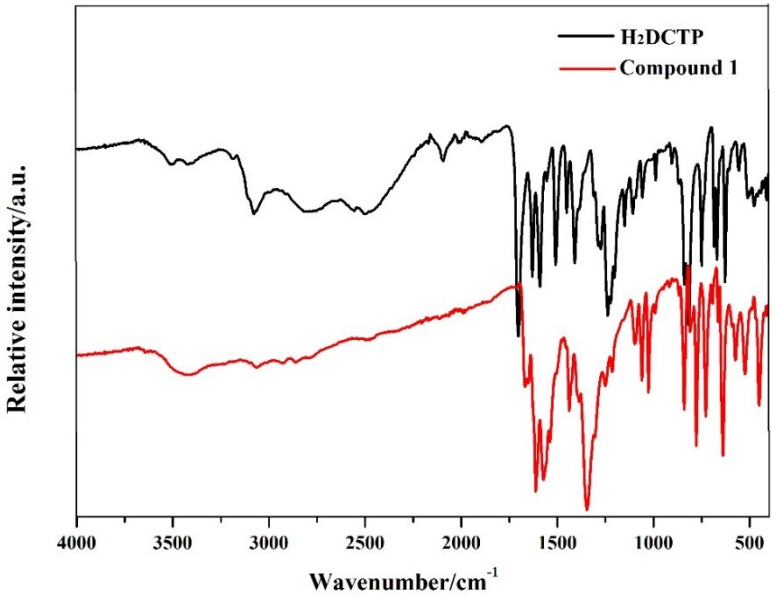

Figure S1. The FT-IR spectra of the ligand (black) and the compound 1 (red).

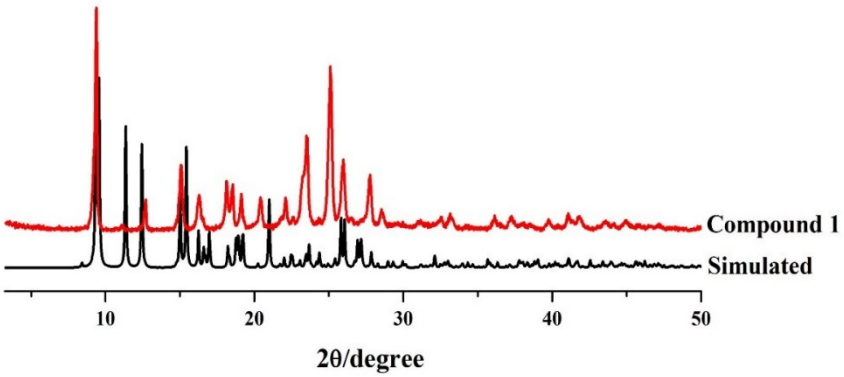

Figure S2. The PXRD patterns of **1**, synthesized compounds (red) and simulated from the single-crystal data (black).

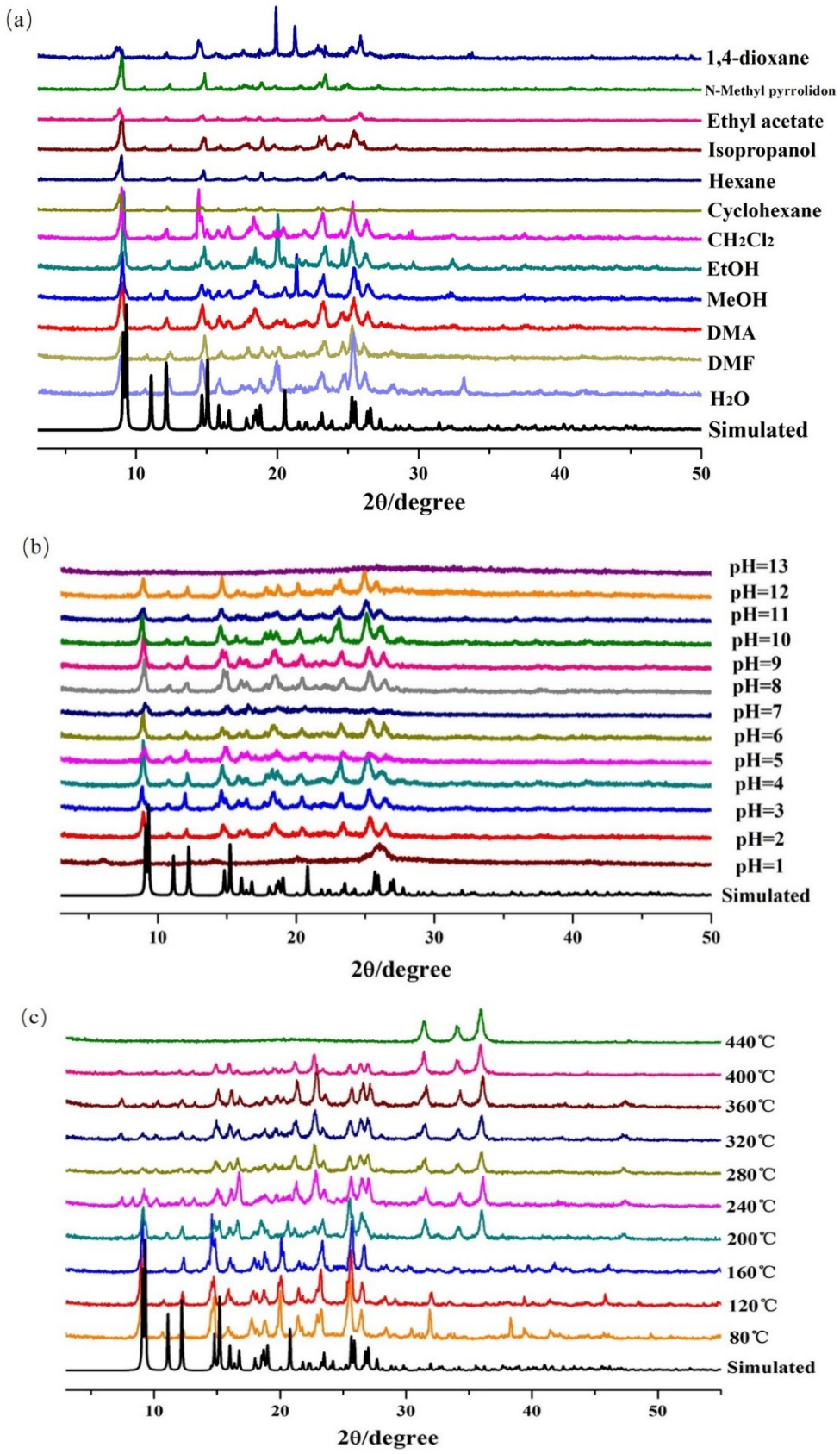

Figure S3. The PXRD patterns of compound **1** after immersing in various organic solvents (a) and different pH values from 1.0 to 13.0 (b); the PXRD patterns of compound **1** after heating at different temperatures (c).

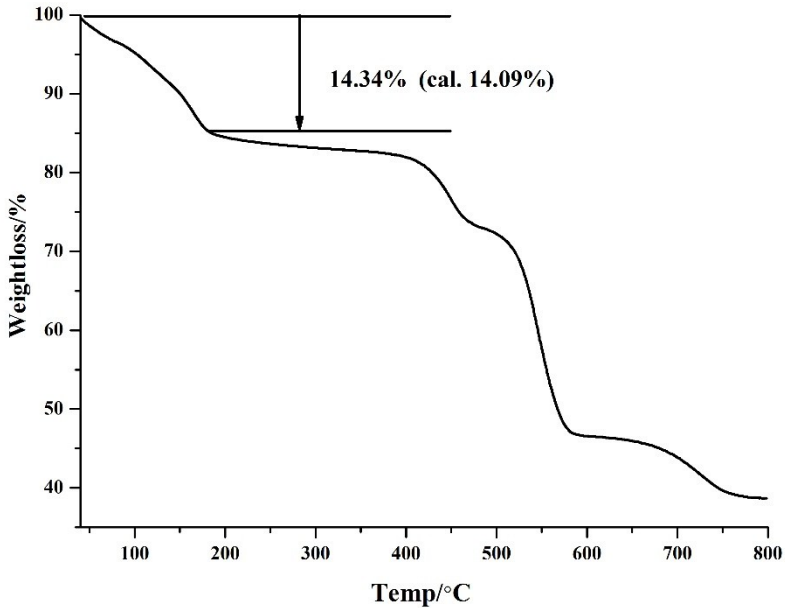

Figure S4. The thermogravimetric analyses curve of compound **1**, the weight loss of 14.34% is similar to the calculated value (14.09%).

4-Butyl-1,3-dioxolan-2-one

^{1}H NMR (300 MHz, $CDCl_3$)

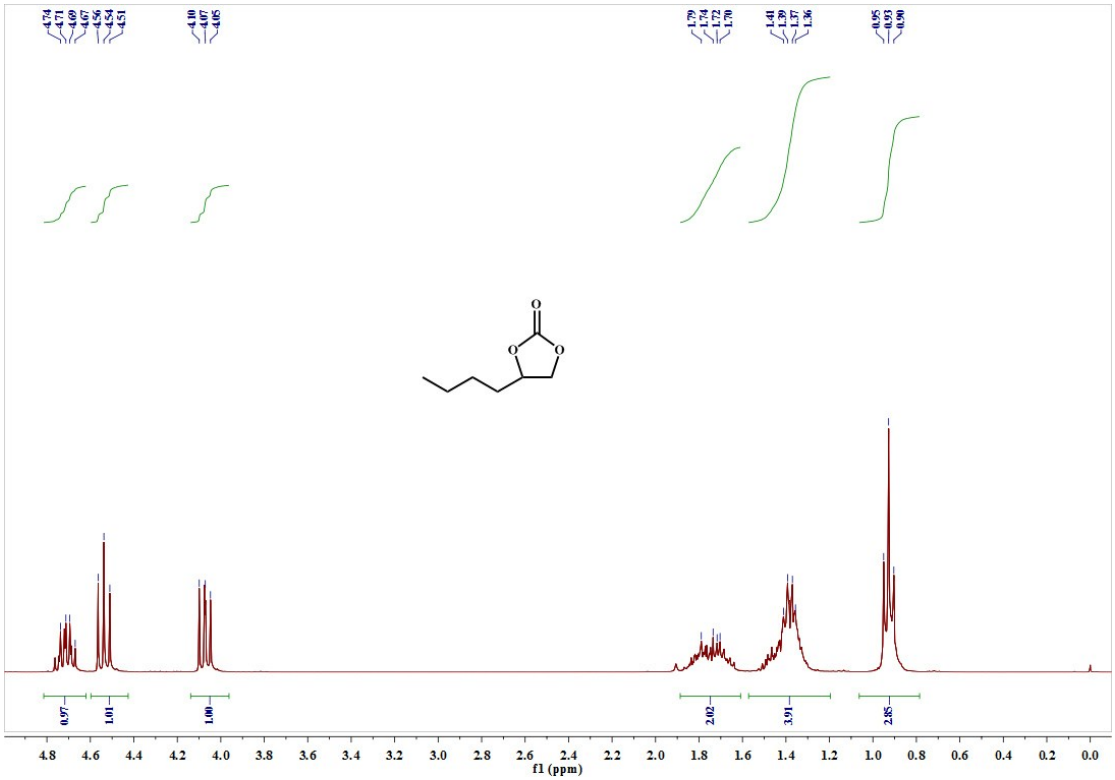

4-Phenyl-1,3-dioxolan-2-one

^{1}H NMR (300 MHz, $CDCl_3$)

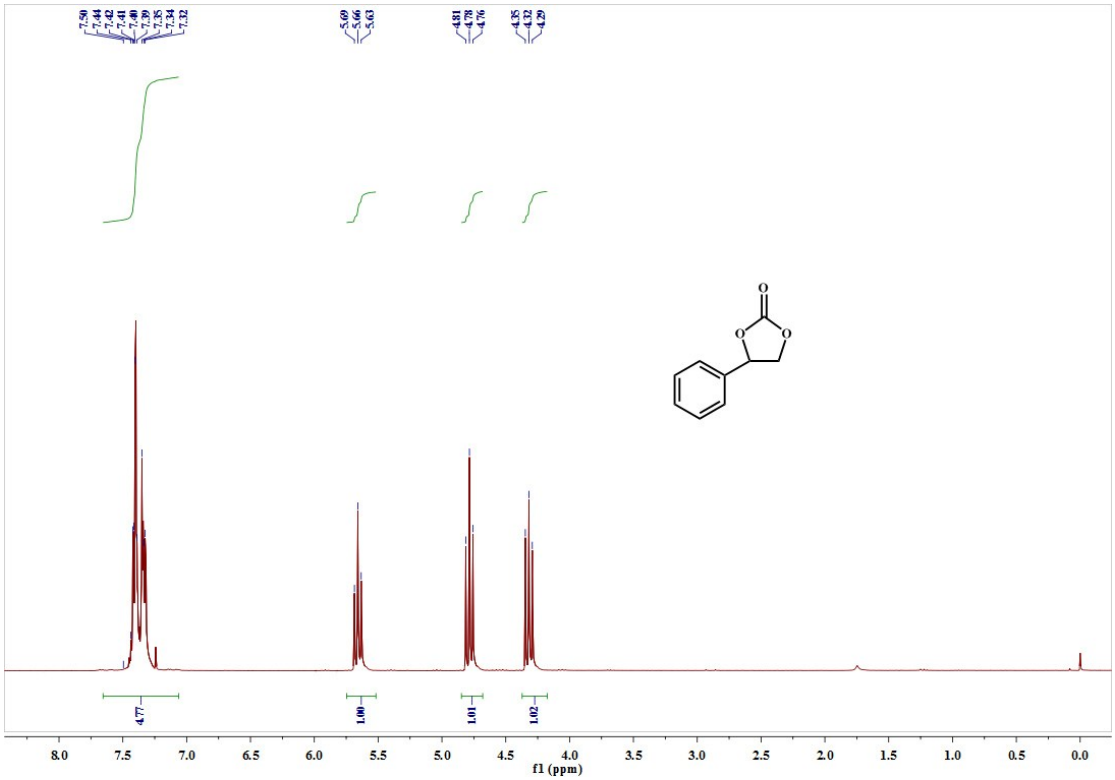

4-(Phenoxymethyl)-1,3-dioxolan-2-one

^{1}H NMR (300 MHz, $CDCl_3$)

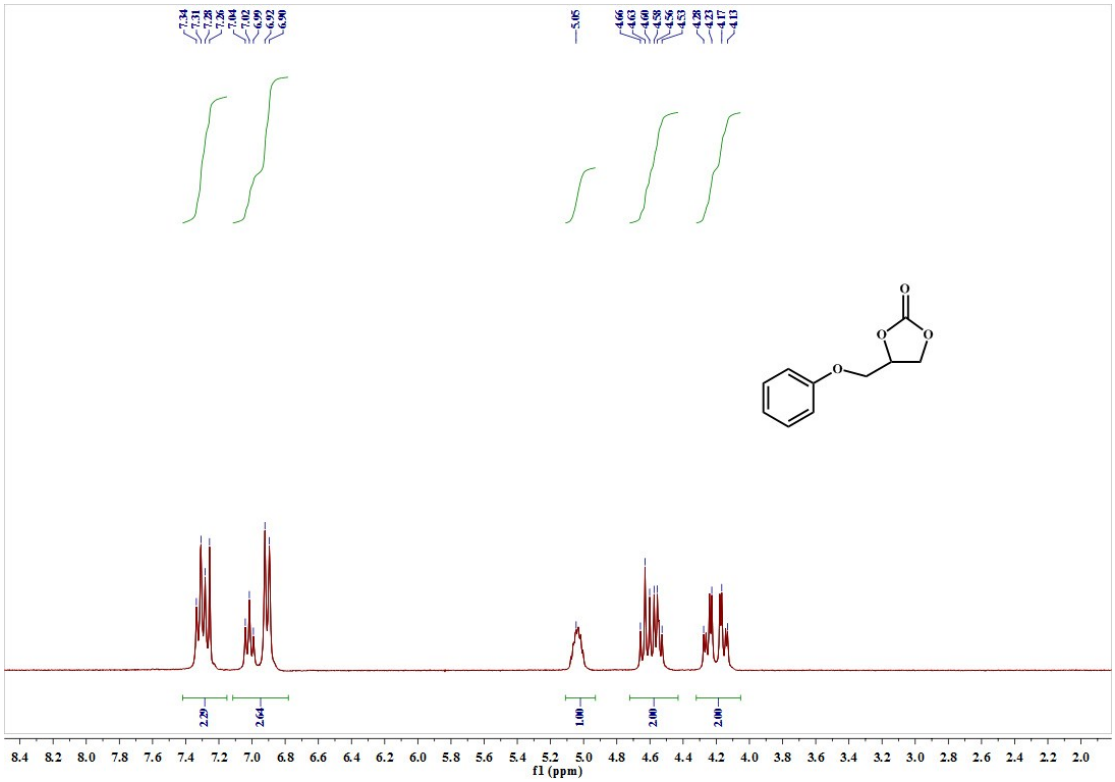

4-(Chloromethyl)-1,3-dioxolan-2-one

^{1}H NMR (300 MHz, $CDCl_3$)

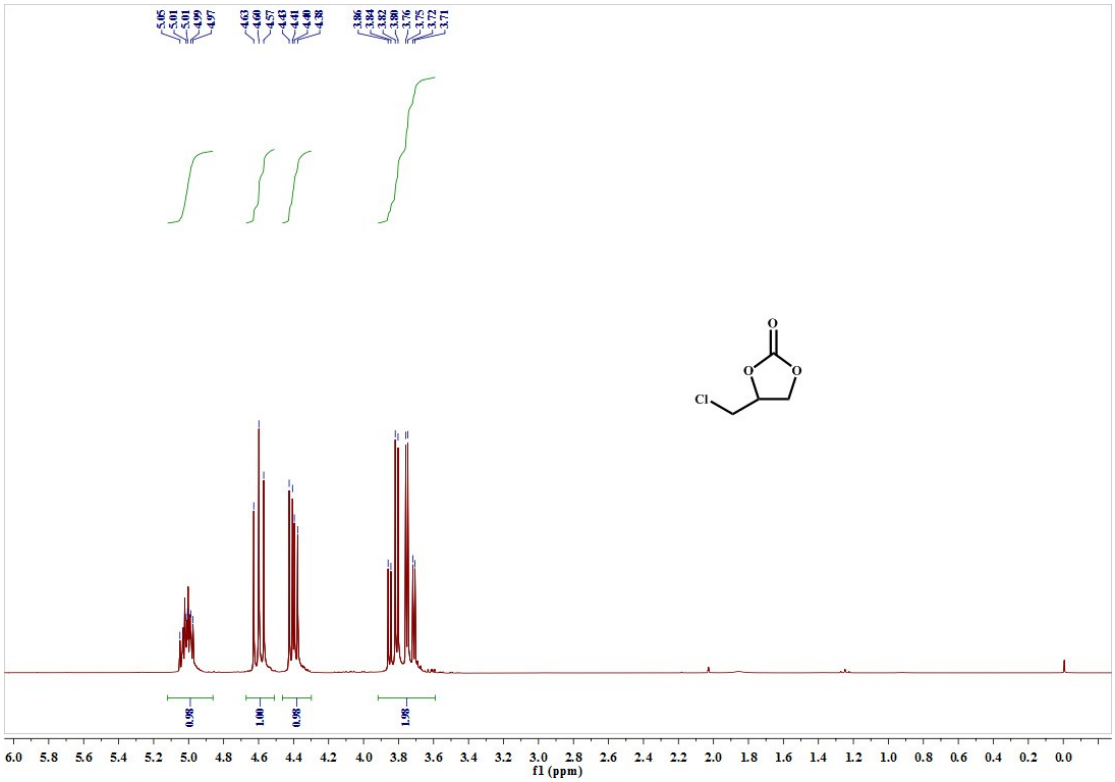

Figure S5. The ^{1}H NMR plots of the products converting from the cycloaddition reaction of CO_2 with epoxides.

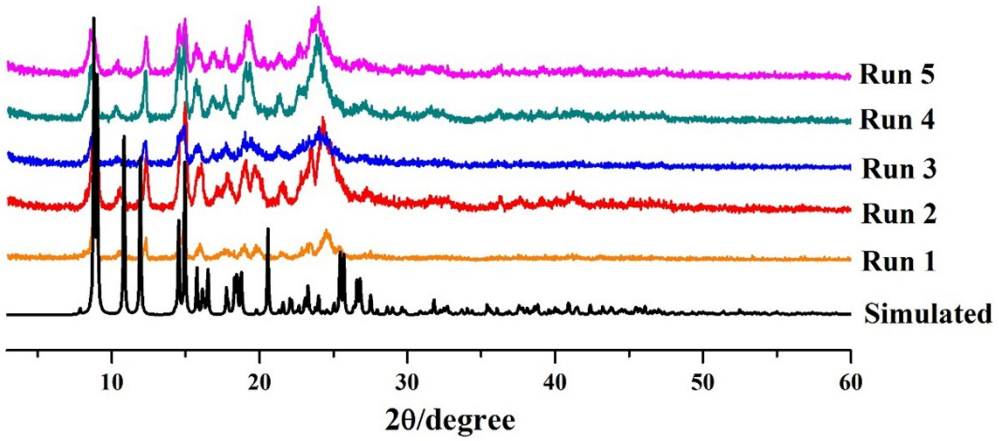

Figure S6. The PXRD patterns of **1** after five catalytic recyclings and the simulated one from **1**.

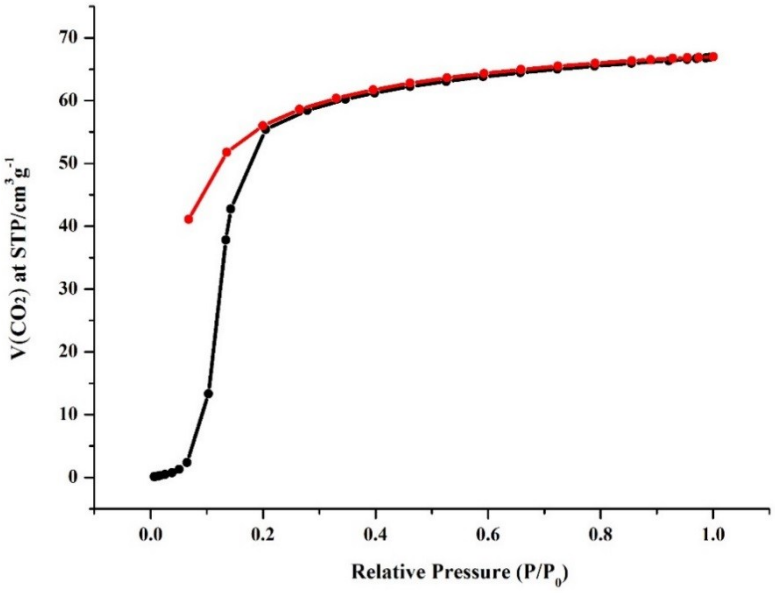

Figure S7. The CO_2 adsorption/desorption of **1** at 273 K.

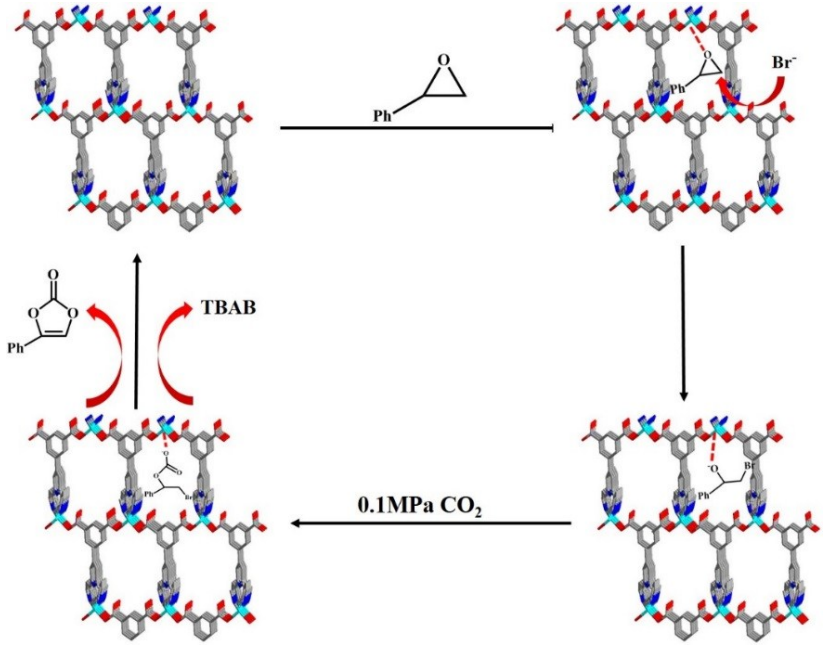

Figure S8. The possible mechanism for the reaction of epoxidation.

Table S2. Comparison of the catalytic activity of some reported interpenetrated-MOFs for the cycloaddition reaction of CO_2 with epoxides.

entry	catalyst	interpenetrated numbers	catalyst (mol %)	pressure (Mpa)	temp (℃)	time (h)	conversion (%)	ref
1[a]	$[\{Ni(muco)(bpa)(2H_2O)\}\cdot 2H_2O]$	3-fold	0.5	0.8	80	12	81.3	1
2[a]	$[\{Co(muco)(bpa)(2H_2O)\}\cdot 2H_2O]_n$	3-fold	0.5	0.8	80	12	>99	2
			0.5	0.1	80	12	85.6	
			0.5	0.1	100	15	94.2	
3[a]	$[Zn_6(TATAB)_4(DABCO)_3(H_2O)_3]\cdot 12DMF\cdot 9H_2O$	3-fold	0.42	0.1	100	16	90	3
4[a]	$\{[Zn(DCTP)]\cdot 3H_2O\}_n$	2-fold	2.8	0.1	70	12	88	this work
5[a]	$[Zn_4OL_3]_n$	2-fold	0.3	0.1	50	4	55	4
6[b]	MMPF-18	4-fold	0.25	0.1	r.t.	48	96.97	5
7[b]	$[Cu(bpy)_2(EDS)]_n$	2-fold	1.0	0.1	r.t.	48	>99	6
8[b]	$\{Cu_2((C_{57}H_{36}N_{12})(COO)_4)(H_2O)_2\cdot 22(DMF)\}_n$	2-fold	0.4	0.1	r.t.	60	94	7
	$\{Cu_2((C_{57}H_{36}N_{12})(COO)_4)(H_2O)_2\cdot 7(DMF)\}_n$	4-fold	0.4	0.1	r.t.	60	49	

[a] The epoxide is styrene oxide, [b] The epoxide is propylene oxide.

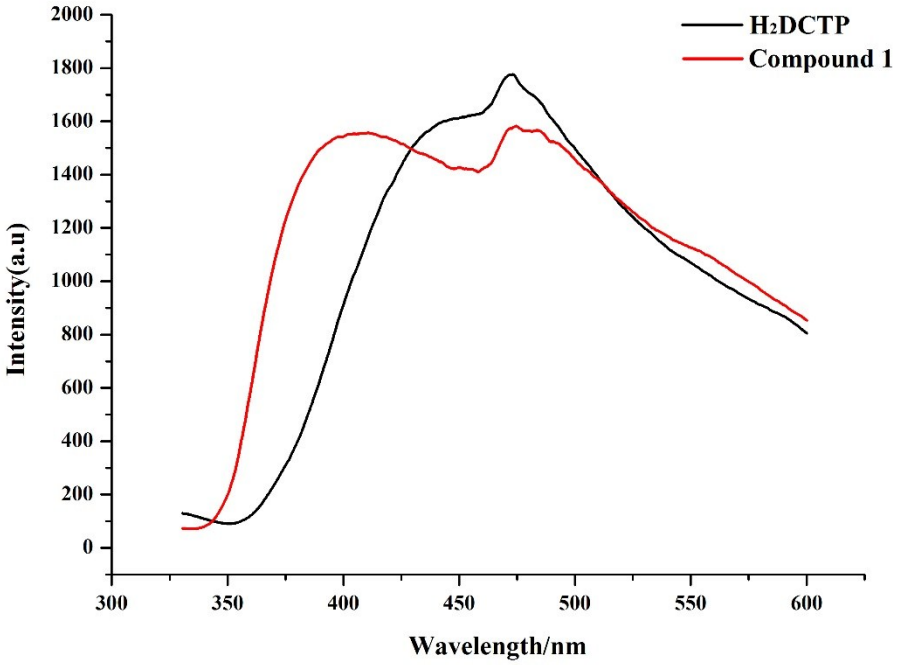

Figure S9. The solid-state photoluminescence spectra of H_2DCTP ($\lambda_{excited}$= 320 nm) and the emission spectra of compound **1** ($\lambda_{excited}$= 320 nm).

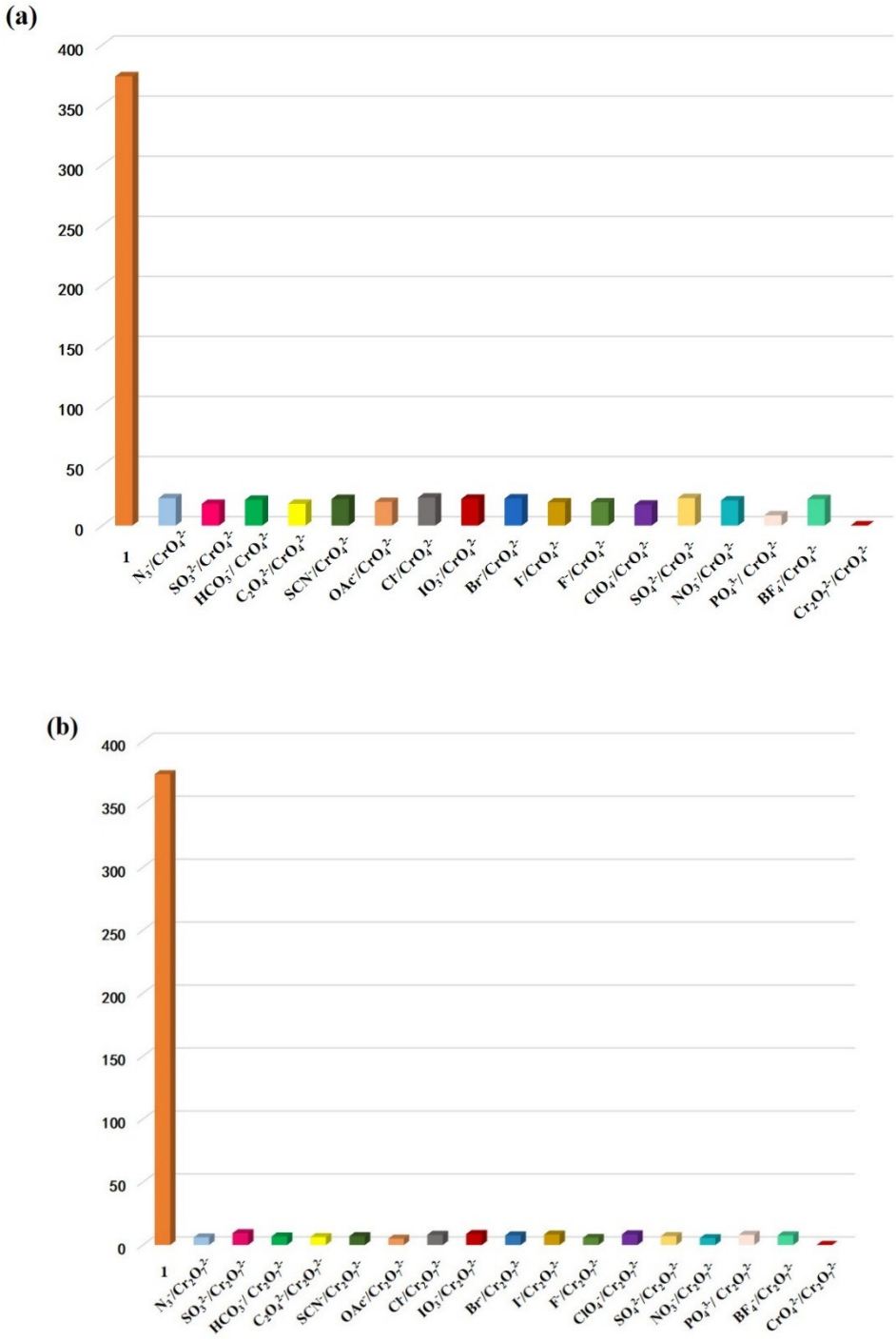

Figure S10. The luminescence intensity of **1**-CrO_4^{2-} (a) and **1**-$Cr_2O_7^{2-}$ (b) under mixed anions (5×10^{-3} M).

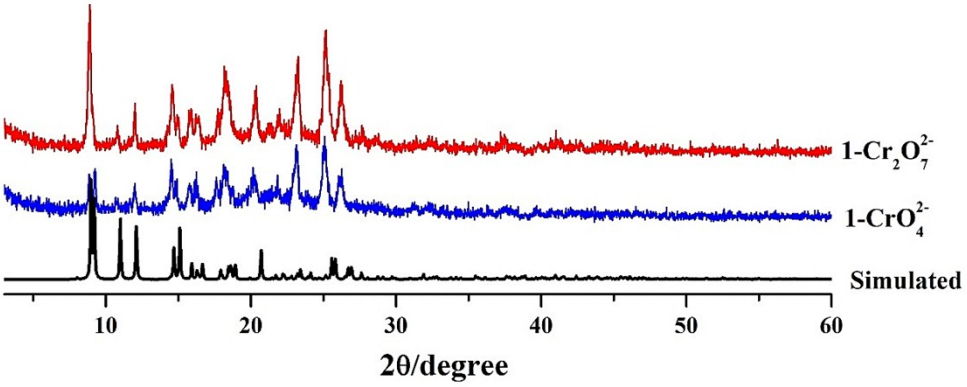

Figure S11. The PXRD patterns of **1** after five luminescent recyclings and the simulated one from compound **1**.

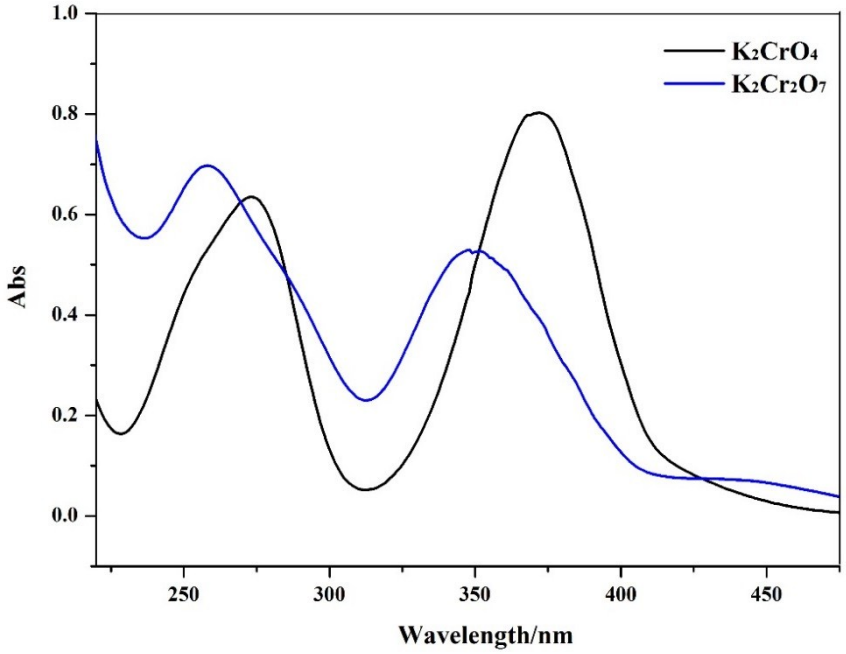

Figure S12. The UV-vis spectra of the K_2CrO_4 and $K_2Cr_2O_7$ solutions.

Table S3. Comparison of the detective limit in some reported CrO_4^{2-}/$Cr_2O_7^{2-}$ sensors.

entry	molecular formula	analyte(CrO_4^{2-}/$Cr_2O_7^{2-}$)	LOD(mol/L)	ref
1	$[Y(BTC)(H_2O)_6]_n$:0.1Eu	CrO_4^{2-}/$Cr_2O_7^{2-}$	3.0×10^{-8}/4.0×10^{-8}	8
2	Eu^{3+}@MIL-121	$Cr_2O_7^{2-}$	5.4×10^{-8}	9
3	$\{[Tb_4Mn\text{-}(BPDC)_3(\mu_3\text{-}H)_4\text{-}(HCOO)_{1.5}(H_2O)_4]\cdot 2.5OH\cdot 8H_2O\}_n$	$Cr_2O_7^{2-}$	10^{-7}	10
4	$\{[Zn_3(bpanth)(oba)_3]\cdot 2DMF\}_n$	CrO_4^{2-}/$Cr_2O_7^{2-}$	1.54×10^{-6}/2.38×10^{-6}	11
5	$\{[Zn(DCTP)]\cdot 2.5H_2O\}_n$	CrO_4^{2-}/$Cr_2O_7^{2-}$	1.0×10^{-6}/1.5×10^{-6}	this work
6	$[Cd(IPA)(L)]_n$	CrO_4^{2-}/$Cr_2O_7^{2-}$	2.52×10^{-6}/2.26×10^{-6}	12
	$[Zn(IPA)(L)]_n$	CrO_4^{2-}/$Cr_2O_7^{2-}$	1.83×10^{-5}/1.2×10^{-5}	
7	$\{[Zn_3(tza)_2(\mu_2\text{-}OH)_2(H_2O)_2]\cdot H_2O\}_n$	CrO_4^{2-}/$Cr_2O_7^{2-}$	4.0×10^{-6}/1.0×10^{-6}	13
8	$[Zn_2(TPOM)(NH_2\text{–}BDC)_2]\cdot 4H_2O$	CrO_4^{2-}/$Cr_2O_7^{2-}$	4.8×10^{-6}/3.9×10^{-6}	14
9	$\{[Zn(btz)]_n\}$	CrO_4^{2-}/$Cr_2O_7^{2-}$	1.0×10^{-5}/2.0×10^{-6}	15
	$\{[Zn_2(ttz)H_2O]_n\}$	CrO_4^{2-}/$Cr_2O_7^{2-}$	2.0×10^{-5}/2.0×10^{-5}	
10	$\{[Cd(L)(BPDC)]\cdot 2H_2O\}_n$	$Cr_2O_7^{2-}$	3.76×10^{-5}	16
	$\{[Cd(L)(SDBA)(H_2O)]\cdot 0.5H_2O\}_n$	$Cr_2O_7^{2-}$	4.86×10^{-5}	

Table S4. The ICP results of compound **1** after catalytic recyclings (filter liquor) and luminescent recyclings (solid sample), respectively.

	Compound **1**
Compound **1** after recyclings (Zn^{2+} of filter liquor)	0.68 ppm
Compound **1** as CrO_4^{2-} sensor after luminescent recyclings (Cr^{6+} of solid sample)	Below detection limit
Compound **1** as $Cr_2O_7^{2-}$ sensor after luminescent recyclings (Cr^{6+} of solid sample)	Below detection limit

References

1 B. Ugale, S. S. Dhankhar, C. M. Nagaraja, *Inorg. Chem.*, 2016, 55, 9757-9766.

2 B. Ugale, S. S. Dhankhar, C. M. Nagaraja, *Cryst. Growth Des.*, 2017, 17, 3295-3305.

3 Y. H. Han, Z. Y. Zhou, C. B. Tian, S. W. Du, *Green Chem.*, 2016, 18, 4086-4091.

4 J. W. Li, Y. W. Ren, C. R. Qi, H. F. Jiang, *Eur. J. Inorg. Chem.*, 2017, 1478-1487.

5 W. Y. Gao, C. Y. Tsai, L. Wojtas, T. Thiounn, C. C. Lin, S. Q. Ma, *Inorg. Chem.*, 2016, 55, 7291-7294.

6 G. Y. Zhang, G. F. Wei, Z. P. Liu, S. R. J. Oliver, H. H. Fei, *Chem. Mater.*, 2016, 28, 6276-6281.

7 P. Z. Li, X. J. Wang, J. Liu, J. Liang, J. Y. J. Chen, Y. L. Zhao, *CrystEngComm*, 2017, 19, 4157-4161
8 T. W. Duan, B. Yan, H. Weng, *Microporous and Mesoporous Materials*, 2015, 217, 196-202.
9 J. N. Hao, B. Yan, *New J. Chem.*, 2016, 40, 4654-4661.
10 J. Dong, H. Xu, S. L. Hou, Z. L. Wu, B. Zhao, *Inorg. Chem.*, 2017, 56, 6244-6250.
11 Z. Q. Yao, G. Y. Li, J. Xu, T. L. Hu, X. H. Bu, *Chem. Eur. J.*, 2018, 24, 3192-3198.
12 B. Parmar, Y. Rachuri, K. K. Bisht, R. Laiya, E. Suresh, *Inorg. Chem.*, 2017, 56, 2627-2638.
13 T. Q. Song, J. Dong, H. L. Gao, J. Z. Cui, B. Zhao, *Dalton Trans.*, 2017, 46, 13862-13868.
14 R. Lv, J. Y. Wang, Y. P. Zhang, H. Li, L. Y. Yang, S. Y. Liao, W. Gu, X. Liu, *J. Mater. Chem. A*, 2016, 4, 15494-15500.
15 C. S. Cao, H. C. Hu, H. Xu, W. Z. Qiao, B. Zhao, *CrystEngComm*, 2016, 18, 4445-4451.
16 S. G. Chen, Z. Z. Shi, L. Qin, H. L. Jia, H. G. Zheng, *Cryst. Growth Des.*, 2017, 17, 67-72.